Draft Version, May 27, 2011
Preprint typeset using LaTeX style emulateapj v. 8/13/10

BUOYANT MAGNETIC LOOPS IN A GLOBAL DYNAMO SIMULATION OF A YOUNG SUN

Nicholas J. Nelson[1], Benjamin P. Brown[2], Allan Sacha Brun[3], Mark S. Miesch[4], & Juri Toomre[1]

Draft Version, May 27, 2011

ABSTRACT

The current dynamo paradigm for the sun and sun-like stars places the generation site for strong toroidal magnetic structures in the deep interior. Sun spots and analogous spots on sun-like stars are believed to be created by sections of these magnetic structures rising from the deep interior to the photosphere. This transport of magnetic fields in sun-like stars from the seat of the global dynamo to the upper regions of the convection zone plays a crucial role in many current models of the solar dynamo. Here we present the first three-dimensional global magnetohydrodynamic (MHD) simulation where turbulent convection, stratification, and rotation combine to yield a dynamo capable of self-consistently generating and transporting magnetic flux through the convection zone of a sun-like star by means of buoyant magnetic loops. Specifically, this simulation of convection and dynamo action in a spherical shell with solar stratification but rotating three times faster than the current solar rate (as our sun did when it was younger and as do many solar analogues) produces strong wreaths of toroidal magnetic field which interact with the convective motions. Some of the regions of strongest magnetic field in these wreaths can rise via magnetic buoyancy instabilities and advection by convective giant cells.

1. COUPLING ROTATION, CONVECTION, AND MAGNETISM IN YOUNGER SUNS

The global solar dynamo which creates sun spots is likely to require several dynamical processes operating at various locations in both the solar interior and atmosphere. Turbulent convection coupled with rotation and stratification produces strong differential rotation in the solar convection zone (see Elliot et al. 2000; Miesch & Toomre 2009) as well as amplifying small-scale magnetic fields. In regions of strong, global shear these small-scale fields are organized and amplified into large-scale toroidal structures through the Ω-effect. The large-scale poloidal field is regenerated through what is known as the α-effect, which may result from small-scale turbulent correlations in the deep interior or through the reconnection of tilted magnetic fields in the solar atmosphere, is less well understood. Portions of the large-scale toroidal magnetic structures are believed to undergo buoyancy instabilities and form loops of magnetic field. The loops then coherently rise through the convective region and pierce the photosphere, forming active regions. In many dynamo models, such as the Babcock-Leighton model (see Charbonneau 2005), the transport of magnetic flux via buoyant loops is a fundamental aspect of the dynamo mechanism.

A single numerical simulation that extends from the deep interior to the solar atmosphere is intractable with current computational resources. Various simulations have studied elements of dynamo action in the sun or sun-like stars. The models of Fan et al. (2003), Abbett et al. (2004), Fan (2008), and Weber et al. (2011) track the rise of flux tubes from the base of the convection zone to the top of the simulated domain. In a similar vein, Jouve & Brun (2009) impose twisted toroidal magnetic structures on a simulation with established convective patterns and solar-like differential rotation and then simulate the rise of magnetic fields as they interact with, and in some cases suppress, turbulent convection. Local dynamo models rely on an imposed shear profile in local Cartesian geometry to drive dynamo action, which can then create buoyant magnetic loops, but the shear in these models in not generated self-consistently by the convection itself; rather it is imposed by a prescribed mechanical forcing. Local dynamo simulations also lack correct global geometry and the properties of the dynamo are very sensitive to the imposed shear profile (e.g. Brummell et al. 2002; Cline et al. 2003; Cattaneo et al. 2006; Guerrero & Käpylä 2011). Global convective MHD simulations incorporate the rotating spherical-shell geometry needed to capture the generation of differential rotation and meridional circulation through Reynolds stresses and anisotropic convective heat transport. Global convective dynamo models have captured the formation of global-scale magnetic structures and cycles in solar and rapidly-rotating sun-like stellar models (e.g., Brown et al. 2010, hereafter B10; Brown et al. 2011, hereafter B11; Ghizaru et al. 2010), which have yielded differential rotation, dynamo action, and large-scale magnetic fields, but not the transport of buoyant magnetic loops towards the top of the convective layer.

In this letter we report on a global convective dynamo simulation of a sun-like star rotating at three times the solar rate $3\Omega_0$, such as our sun when it was younger. This simulation is capable of modeling (1) a solar-like differential rotation profile created by the interplay of convection, rotation, and stratification, (2) the formation of global-scale toroidal magnetic structures that undergo cycles of magnetic activity and reversals of global polarity, and (3) the creation of buoyant magnetic loops from the strongest portions of the toroidal structures which

[1] JILA and Dept. Astrophysical & Planetary Sciences, University of Colorado, Boulder, CO 80309-0440
[2] Dept. Astronomy, University of Wisconsin, Madison, WI 53706-1582
[3] DSM/DAPNIA/SAp, CEA Saclay, 91191 Gif-sur-Yvette, France.
[4] High Altitude Observatory, NCAR, Boulder, CO 80307-3000

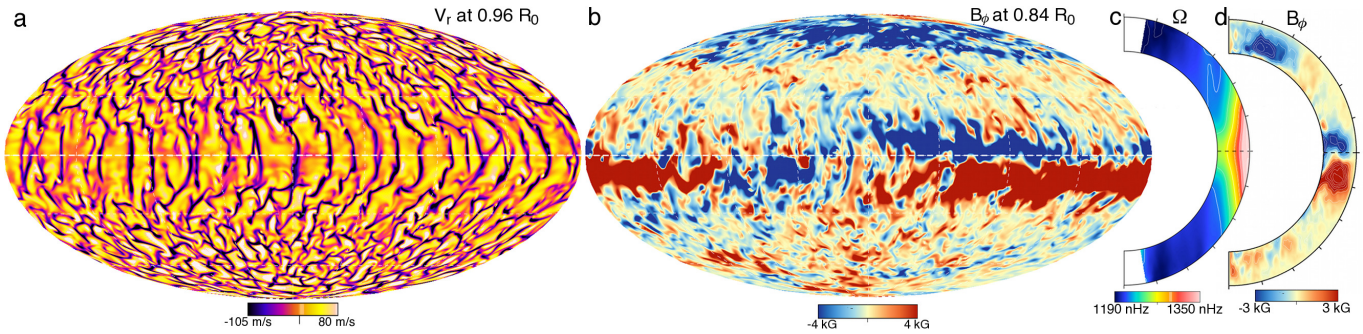

FIG. 1.— (*a*) Radial velocity in global Mollweide projection near the top of the computational domain with fast, narrow downflows in dark tones and broad, slower upflows in light tones. (*b*) Companion Mollweide projection of B_ϕ at mid-convection zone. Here the strong effects of turbulent convection are seen in the ragged nature of the wreaths. Several buoyant magnetic loops (see Fig. 3) are generated in the negative-polarity wreath segment just above the equator and right of image center. (*c*) Time-averaged mean rotation profile, showing faster-rotating equatorial region with slower rotation at higher latitudes. (*d*) Mean toroidal magentic field at the same time as *a* and *b*. Even though the wreaths appear limited in longitudinal extent they still have strong mean-field signatures.

rise from the base of the convection zone to near the upper boundary of our simulation. This work extends the work of B10 in which a simulation at $3\Omega_0$ with moderate levels of diffusion was able to accomplish (1) and (2). The formation of buoyant loops (3) if facilitated in our current work by a dynamic Smagorinsky subgrid-scale model (Germano et al. 1991), serve to minimize the overall levels of diffusion in a simulation at a given spatial resolution.

2. SIMULATION PARAMETERS AND PROPERTIES

We have conducted 3-D MHD simulations of turbulent convection and dynamo action in a spherical shell rotating at $3\Omega_0$, or once every 9.3 days, using the anelastic spherical harmonic (ASH) code (Clune et al. 1999; Brun et al. 2004). ASH is a Large-Eddy Simulation (LES) code that resolves the largest scales of motion and uses a subgrid-scale (SGS) model to parameterize the effects of unresolved, small-scale turbulence. The dynamo simulations of B10 and B11 use an SGS model where the turbulent magnetic diffusivity η_t is constant on spherical shells and in time, and varies only slowly with depth as the inverse square-root of the background density. We will call this SGS treatment the enhanced mean eddy viscosity model. B10 examined a simulation (labeled case D3) at $3\Omega_0$ which exhibited persistent toroidal magnetic structures, while B11 studied a simulation that achieved cycles of magnetic activity and global polarity reversals at $5\Omega_0$ (labeled case D5). Both simulations had $\eta_t \approx 2 \times 10^{12}$ cm^2/s at mid-convection zone.

Here we present a global ASH dynamo simulation of a star with solar stratification rotating at $3\Omega_0$ which has its lower boundary at 0.72 of the solar radius R_0 and its upper boundary at 0.97 R_0. This simulation, which we label case S3, is able to achieve very low levels of viscous, thermal, and magnetic diffusion through the use of a dynamic Smagorinksy SGS model. The dynamic Smagorinsky SGS model relies on an assumption of self-similar behavior in the resolved portion of the inertial range of scales in a turbulent flow to extrapolate the effects of unresolved small-scale motions on the resolved scales. This results in a viscosity ν_S that varies by orders of magnitude in all three spatial dimensions and in time, and is determined by the properties of the grid and the flows, the only free parameter being the so-called test scale ℓ_t, which represents the smallest spherical harmonic degree (largest length scale) in the inertial range. Here we set $\ell_t = \ell_{max}/2 = 170$. We assume constant thermal and magnetic Prandtl numbers, which in case D3, D5, and S3 are set to 0.25 and 0.5 respectively, to determine the thermal and magnetic diffusion coefficents. We reserve further discussion of the properties of ASH simulations using the dynamic Smagorinsky SGS model for a forthcoming paper. In case S3 the dynamic Smagorinsky SGS model allows a simulation with 1024 longitudinal, 512 latitudinal, and 193 radial grid points to achieve a mean magnetic diffusion coefficient at mid-convection zone of $\bar{\eta}_t = 4.8 \times 10^{10}$ cm^2/s. This reduction in diffusion by a factor of about 40 from case D3 is critical for the formation and coherent rise of buoyant magnetic loops.

Case S3 exhibits highly turbulent convective patterns shown in Figure (1a) which are largely vortical at high latitudes and aligned with the rotation axis near the equator. The convection builds and maintains a strong differential rotation that is prograde at the equator and retrograde at mid- to high-latitudes (Fig. 1c). This strong, organized shear drives the creation of toroidal magnetic structures at low-latitudes in each hemisphere through the Ω-effect, as demonstrated in B10. Here, however, the increased levels of turbulence limit the magnetic wreaths to smaller longitudinal extents, as shown in Figure (1b), while still maintaining a strong signature in the azimuthally-averaged toroidal field $\langle B_\phi \rangle_\phi$ (Fig. 1d).

In addition to creating strong magnetic structures near the base of the convective region, case S3 also undergoes cycles of magnetic activity and reversals of global magnetic polarity similar to those described in case D5 in B11. Because of the large computational cost of the dynamic Smagorinsky SGS model, case S3 was started using a descendent of case D3 (which we call case D3b) as initial conditions (see Nelson et al. 2010). Case D3b uses the enhanced mean eddy diffusion model used in cases D3 and D5, but at higher resolution and corresponding lower levels of diffusion ($\eta_t = 8.9 \times 10^{11}$ cm^2/s at mid-convection zone) while holding all other parameters constant. The temporal evolution of the hemispherically-averaged toroidal magnetic field $\langle B_\phi \rangle$ in case D3b over roughly 5000 days is shown in the upper panel of Figure (2), demonstrating the irregular cycles this model yields. Case S3 continues this behavior over roughly 1300 simulated days. The temporal evolution of $\langle B_\phi \rangle$ in case

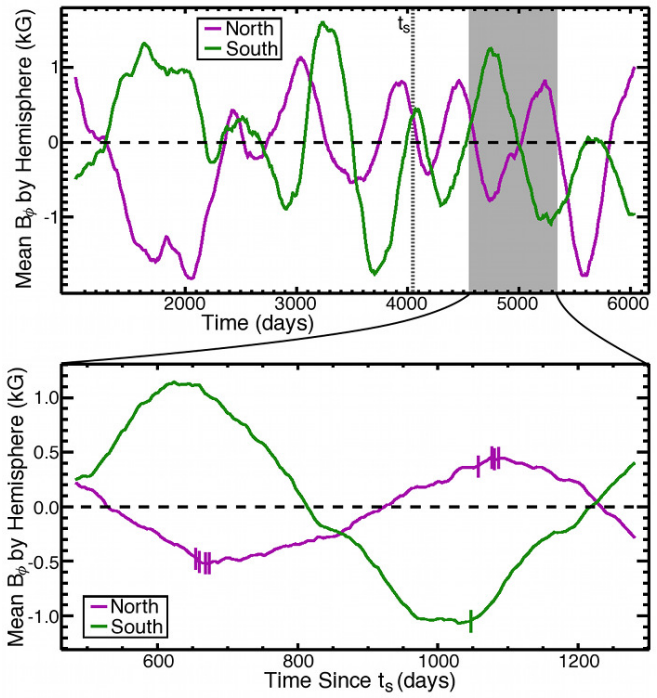

FIG. 2.— Volume-averaged toroidal magnetic field in each hemisphere of the case D3b over nearly 6000 days (top panel) and of case S3 over about 800 days (bottom panel). Case S3 began using case D3b at time t_s (indicated by dotted line) as initial conditions. Case S3 continues the cyclic behavior of its progenitor, but is additionally capable of producing buoyant loops. The creation of loops which reach or exceed $0.90R_0$ are indicated by tick marks in the lower panel.

S3 is shown in the lower panel of Figure (2), revealing two reversals of global magnetic polarity. Similar reversals are seen when examining the hemispherically-averaged poloidal field, the dipole moment, and the polarity of the strongest toroidal structure in each hemisphere.

For the purposes of this paper, we will discuss only buoyant magnetic structures which coherently rise above $0.90R_0$ while remaining connected to the large-scale toroidal wreaths. We have identified nine buoyant magnetic loops which meet this definition which are indicated as hash marks on the bottom panel of Figure (2). Eight loops are seen in the northern hemisphere and one is seen in the southern hemisphere.

3. BUOYANT MAGNETIC LOOPS

Buoyant magnetic loops begin as the cores of strong toroidal magnetic wreaths which are created near the base of the simulated domain. While these wreaths have strong $\langle B_\phi \rangle_\phi$ components that peak around 5 kG, they are generally not axisymmetric structures in case S3. This is a change from the largely axisymmetric wreaths seen in case D3 at $3\Omega_0$ with persistent wreaths (B10) or case D5 at $5\Omega_0$ with wreaths that undergo cyclic reversals in magnetic polarity (B11). In case S3 the wreaths are strong, coherent structures over as little as 60° to as much as 300° of longitude. For example, Figure (1b) shows a negative polarity wreath in the northern hemisphere spanning 95° in longitude while a positive polarity wreath in the southern hemisphere extends over nearly 270° in longitude. The longitudinal sizes of the wreaths vary over the magnetic activity cycle, but generally the wreaths are longest near cycle maximum. If we define the wreaths as contiguous volumes with $|B_\phi| > 4$ kG then we can compute geometric properties of the wreaths in latitude and radius at cycle maximum. Averaging over the four instances simulated in this fashion, we find that the wreaths extend between equator and ±15° of latitude and between the bottom boundary at $0.72R_0$ and $0.86R_0$. If we take an average weighed by magnetic field strength, we find that the mean center of the wreaths is located at ±7° latitude and $0.755R_0$ in radius. On average the wreaths cover 26% of the cross-sectional area in the domain between the equator and ±30° latitude. The average magnetic field strength in the wreaths starts at 12.7 kG at the base of the domain, decreases linearly moving upward in radius to 4.6 kG at $0.75R_0$, and is roughly constant until the top of the wreath is nearly reached at $0.85R_0$. Above that the average magnetic field strength again decreases linearly to below the cut-off value of 4 kG at $0.86R_0$.

As demonstrated in cases D3 (B10) and D5 (B11), the wreaths are highly non-uniform and display strong internal variation as well as a high degree of connectivity with the rest of the domain. Magnetic field lines regularly leave and enter the wreaths. Portions of the wreaths can have significantly higher field strengths and some portions show enhanced organization of field lines. In case S3 portions of the wreaths covering between 20° and 80° of longitude can have coherent cores where B_ϕ can regularly exceed 30 kG and reach values as high as 45 kG. In these cores, bundles of magnetic field lines show very little local connectivity with the rest of the domain or even the other potions of the wreath. As $\langle B_\phi \rangle$ increases, both the longitudinal extent and peak B_ϕ values of these coherent cores increase. A single wreath of a given polarity may not form a coherent core at all or may have more than one core, and a single core may produce multiple buoyant loops. Of the nine buoyant loops investigated here to extend past $0.90R_0$, one coherent core produces four buoyant loops, another produces three, and two more cores each yield a single buoyant loop.

Some, but not all, of the coherent wreath cores can become what we term buoyant magnetic loop progenitors or proto-loops. In these proto-loops the ratio of magnetic to kinetic energy densities regularly exceeds 100, resulting in highly suppressed convective motions from strong Lorentz forces. Without strong, small-scale advection and turbulent mixing, the proto-loops become even stronger and more organized under the presence of large-scale shear from the differential rotation. When magnetic field strengths approach 45 kG the proto-loops become under-dense as magnetic pressure displaces fluid pressure, causing buoyant acceleration. As the proto-loop rises its magnetic field quickly weakens down to about 20 kG due to expansion and diffusion. After rising 2% to 3% of the solar radius, the proto-loop can enter a region where strong convective giant cells are present. These flows advect portions of the proto-loop downward at cell edges and upward in the core of the giant cells. The rise of the top of a magnetic loop is shown in cross-section by sampling B_ϕ roughly every 2 days in Figure (3a).

One way to track these buoyant loops is to use 3-D tracings of magnetic field lines. In our simulations with finite resistivity, individual field lines do not maintain their identity over time, however one can achieve some

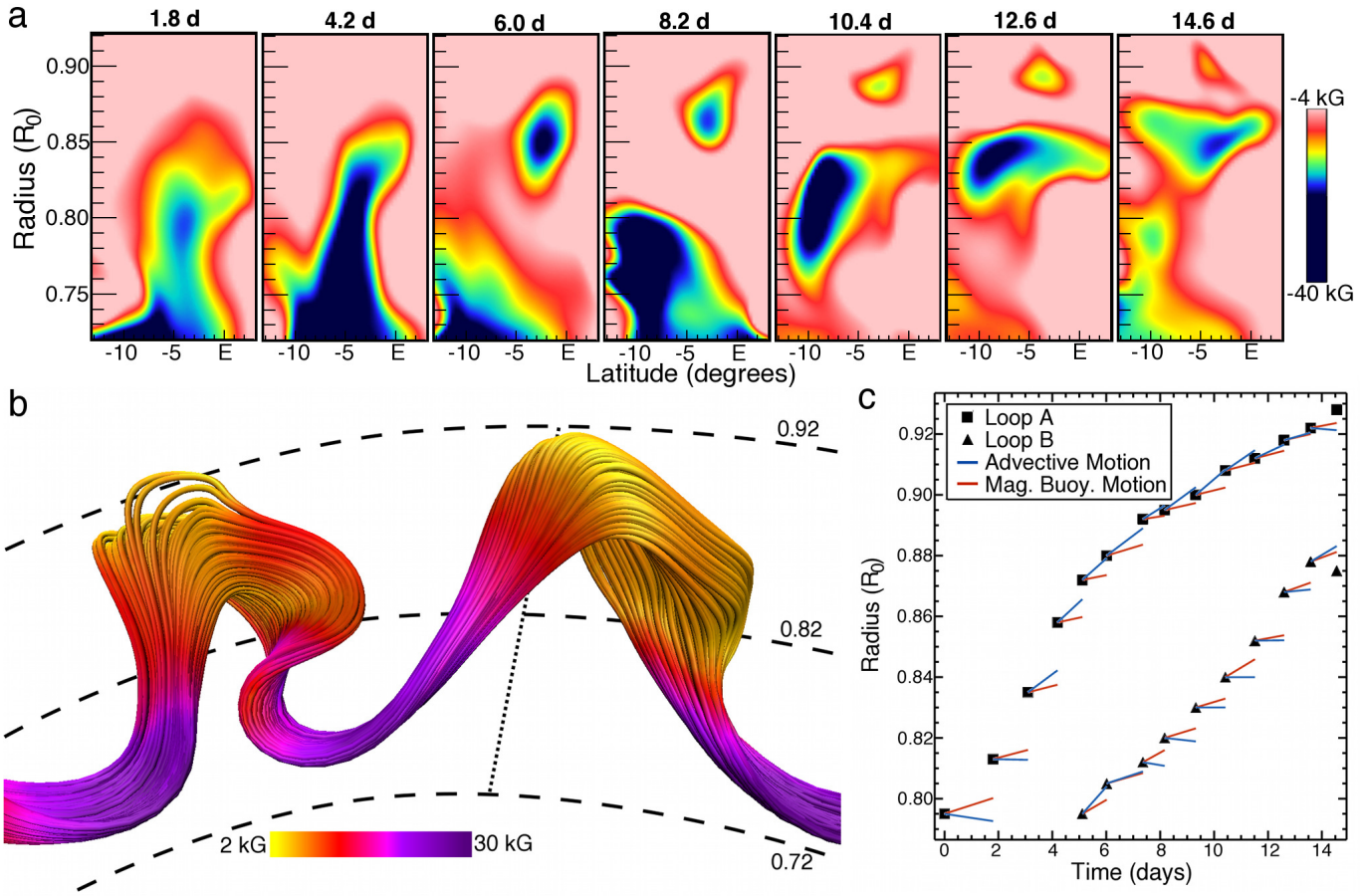

FIG. 3.— (a) 2-D cuts in longitude at sucussive times as indicated showing toroidal magnetic field over radius and latitude. The rising magnetic loop is seen in cross-section starting at $0.81R_0$ at $t = 0$ days and rising to $0.91R_0$ after roughly 15 days. A second loop is also seen rising starting at 8.6 days, however the top of this second loop never rises above $0.88R_0$. (b) 3-D visualization of magnetic field lines in the core of a wreath which produces four loops (two shown here) at day 14.6 (rightmost panel of a, rightmost symbol of c, Figs. 1a-b). Perspective is looking down along the rotation axis towards the equatorial plane. The right loop is the upper loop in a and "Loop A" in c. Coloring indicates $|\vec{B}|$. Dashed lines indicate radial position. Dotted line shows the cutting plane used in the left-most panel of a. The loops remain coherently connected to the very strong ($\approx$ 40 kG) fields which are pinned near the base of the convective zone by fast downflows. (c) Radial location of the top of a buoyant loop as a function of time, along with the movement due purely to magnetic buoyancy (red lines) and advection by convective upflows blue lines).

measure of consistency when moving in time by tracking bundles of magnetic field lines. We assume that the very strong fields at the bottom of the loops near the base of the domain maintain their identities in time and so we randomly seed large numbers (here we use 1000) field lines in those strong footpoints at each time step. Thus while any given field line may not maintain its identity between time steps, the average over many field lines approximately does. Figure (3b) shows 3-D renderings of magnetic fields lines for two sample loops near the peak of their rise. Similar field line tracings have been studied at various times during the rise of these loops.

At maximum size the magnetic loops extend from $0.73R_0$ to $0.93R_0$. The magnetic fields exceed 30 kG at the base of the loops near $0.72R_0$ but become much weaker near the tops of the loops, with field strengths as low as 5 kG. The loops are embedded in the much larger wreaths which have an average cross-sectional area of 13800 Mm^2. The cross-sectional area of the loop shown in Figures (3a-c) is 120.2 Mm^2 at the starts of its rise at $0.795R_0$ and 520.0 Mm^2 at its peak radial position of $0.927R_0$. Accounting for the continued expansion that would likely occur if this loop were able to continue rising, the cross-sectional area is reasonable compared with the typical area of a large sunspot at the photosphere, which is roughly 2500 Mm^2 (Zwaan 1987). If the loop's rise were adiabatic, the cross-sectional area should change in inverse proportion to the change in background pressure, which decreases by a factor of 17.1, rather than the observed expansion by a factor of 4.3. The top of the loop must then have a net outflow of either heat or material in order to avoid expanding adiabatically. The loops show a measurable deficit in density and thermodynamic pressure relative to their surroundings, but they do not present any signature in temperature or entropy. This indicates that they are thermally "leaky" and able to equilibrate with their surroundings quickly compared to the timescale for radial motion. This is interesting since a simple estimate of the diffusion time across one of these structures at mid-convection zone is on the order of 50 days, implying that there is a divergent flow at the top of the loop, moving fluid along field lines.

Once a loop has begun to rise, its radial motion is dominated by advection and magnetic buoyancy. Fig-

ure (3c) illustrates the rise of a sample magnetic loop while also indicating the components of the motion due to advection and magnetic buoyancy. To compare motion due to magnetic buoyancy, we integrate the magnetically buoyant acceleration over time between the times sampled in Fig. (3c) (time intervals of approximately 2 days) to compute an average velocity at each time due to magnetic buoyancy. The advective velocity is simply the volume-averaged velocity of the surrounding fluid. Initially the sample proto-loop experiences an upward velocity due to magnetic buoyancy of 46.1 m s^{-1} compared to a downward motion of the surrounding fluid at an average rate of -10.8 m s^{-1}. After 3 days of movement dominated by magnetic buoyancy, the loop gets caught up in a convective updraft and the velocity of the surrounding fluid becomes larger than the velocity from buoyant acceleration. Even though advective motions dominate, magnetic buoyancy continues to drive upward motion of between 22.2 and 34.9 m s^{-1} relative the surrounding fluid. Thus, magnetic buoyancy and convection work in concert to promote the rise of the loop. Continued buoyant acceleration as the magnetic pressure weakens is achieved by the density perturbation of the loop falling off at roughly the same rate as the background density stratification. Once the top of the loop has entered the main convective upflow it experiences advection at between 45.1 and 66.4 m s^{-1} until 11.5 days when the upflow begins to slow, reaching 7.0 m s^{-1} at 14.6 days. The presence of strong magnetic buoyancy forces allow this loop to rise in 14.6 days while the average upflow traverses the same distance in 21.7 days and magnetic buoyancy alone would require 30.6 days.

Additional accelerations are present but not plotted, including thermal buoyancy, which is significant early in the rise of the loop, and magnetic tension, which is of the same order of magnitude as the advective motion near maximum radial extent at 14.6 days. Thermal buoyancy is distinguished from magnetic buoyancy by averaging over the convective updraft but excluding regions with magnetic fields stronger than 4 kG. The downward force of magnetic tension may play in role preventing any additional upward motion. In the first several days magnetic diffusion also produces an apparent upward motion as magnetic fields in the center of the wreath diffuse upward. An additional apparent motion at early times is produced as much of the toroidal magnetic field used to track the loops is converted to radial magnetic field in the sides of the loops. Throughout the rise of the loop, however, magnetic buoyancy and advection play dominant roles. Because advection plays a crucial role in the transport of these loops of magnetic field the size scale of the loops is set by the size of the convective giant cells. The nine loops studied here have an average size of 15.4° in longitude when measuring across the bottom of the loop while the average distance between convective downflows in the equatorial region is 16.4° in longitude. Similar dynamics are observed in thin flux tubes subject to a background convective flow (Weber et al. 2011).

In this paper we have presented a 3-D MHD simulation that combines turbulent convection, rotation, and stratification to produce solar-like differential rotation and large-scale toroidal magnetic structures at the base of the convection zone which undergo cycles of magnetic activity and reversals of global magnetic polarity. Most notably these also exhibit buoyant magnetic loops capable of coherently traversing much of the convective layer. To our knowledge, this is the first convection simulation to spontaneously produce buoyant magnetic loops by means of rotational shear that is established and maintained by the convection itself. These buoyant loops which appear at cycle maximum can have toroidal field strengths of 45 kG at their base and 5 kG at their top. Their size scales are set by the size of the convective giant cells and they have cross-sectional areas at $0.90R_0$ that are reasonable compared to the sizes of large sunspots. These buoyant magnetic loops are an essential step toward unifying numerical models of convective dynamos and flux emergence.

REFERENCES

Abbett, W. P., Fisher, G. H., Fan, Y., & Bercik, D. J. 2004, ApJ, 612, 557
Brown, B.P., Browning, M. K., Brun, A. S., Miesch, M. S., & Toomre, J. 2010, ApJ, 711, 424
Brown, B. P., Miesch, M. S., Browning, M. K., Brun, A. S., & Toomre, J. 2011, ApJ, 731, 69
Brown B. P. et al. 2007, in AIP Conf. Ser. 948, Unsolved Problems in Stellar Physics: A Conference in Honor of Douglas Gough, ed. Stancliffe et al. (Melville, NY: AIP), 271
Brummell, N., Cline, K., & Cattaneo, F. 2002, MNRAS, 329, L73
Brun, A.S., Miesch, M.S., & Toomre, J. 2004, ApJ, 614, 1073
Cattaneo, F., Brummell, N. H., & Cline, K. S. 2006, MNRAS, 365, 727
Charbonneau, P. 2005, Living Rev. Sol. Phys., 2, 2
Cline, K. S., Brummell, N. H., & Cattaneo, F. 2003, ApJ, 588, 630
Clune, T.L., Elliot, J.R., Miesch, M.S., & Toomre, J. 1999, Parallel Comput., 25, 361
Elliott, J. R., Miesch, M. S., & Toomre, J. 2000, ApJ, 553, 546
Fan, Y., Abbett, W. P., & Fisher, G. H. 2003, ApJ, 582, 1206
Fan, Y. 2008, ApJ, 676, 680
Germano, M., Piomelli, U., Moin, P., & Cabot, W. 1991, Phys. Fluids A, 3, 7
Ghizaru, M., Charbonneau, P., & Smolarkiewicz, P. K. 2010, ApJ, 715, L133
Guerrero, G., & Käpylä, P. 2011, arXiv:1102.3598
Miesch, M. S. & Toomre, J. 2009, Annu. Rev. Fluid Mech. 41, 317
Nelson, N. J., Brown, B. P., Browning, M. K., Brun, A. S., Miesch, M. S., & Toomre, J. 2010, in Proc. of IAU Symposium 273: The Physics of Sun and Star Spots, ed. Someone et al. (Cambridge: Cambridge University Press), page
Weber, M. A., Fan, Y., & Miesch, M. S. 2011, ApJsubmitted
Zwaan, C. 1987, ARA&A, 25, 83